Cross-talk artefacts in Kelvin probe force microscopy imaging : a comprehensive study

Sophie Barbet, Michka Popoff, Heinrich Diesinger, D. Deresmes, Didier Theron, Thierry Melin

Cross-talk artefacts in Kelvin probe force microscopy imaging: A comprehensive study

Cite as: J. Appl. Phys. **115**, 144313 (2014); https://doi.org/10.1063/1.4870710
Submitted: 22 February 2014 • Accepted: 26 March 2014 • Published Online: 14 April 2014

S. Barbet, M. Popoff, H. Diesinger, et al.

JOURNAL OF APPLIED PHYSICS **115**, 144313 (2014)

Cross-talk artefacts in Kelvin probe force microscopy imaging: A comprehensive study

S. Barbet,[1] M. Popoff,[1,2] H. Diesinger,[1] D. Deresmes,[1] D. Théron,[1] and T. Mélin[1,a)]
[1]*Institute of Electronics, Microelectronics and Nanotechnology, CNRS UMR8520, Avenue Poincaré, F-59652 Villeneuve d'Ascq, France*
[2]*Lille Centre for Infection and Immunity, Cellular Microbiology of Infectious Pathogens, CNRS UMR8204, INSERM U1019, University of Lille Nord-de-France, Institut Pasteur de Lille, F-59019 Lille, France*

(Received 22 February 2014; accepted 26 March 2014; published online 14 April 2014)

We provide in this article a comprehensive study of the role of ac cross-talk effects in Kelvin Probe Force Microscopy (KPFM), and their consequences onto KPFM imaging. The dependence of KPFM signals upon internal parameters such as the cantilever excitation frequency and the projection angle of the KPFM feedback loop is reviewed, and compared with an analytical model. We show that ac cross-talks affect the measured KPFM signals as a function of the tip-substrate distance, and thus hamper the measurement of three-dimensional KPFM signals. The influence of ac cross-talks is also demonstrated onto KPFM images, in the form of topography footprints onto KPFM images, especially in the constant distance (lift) imaging mode. Our analysis is applied to unambiguously probe charging effects in tobacco mosaic viruses (TMVs) in ambient air. TMVs are demonstrated to be electrically neutral when deposited on silicon dioxide surfaces, but inhomogeneously negatively charged when deposited on a gold surface.
[http://dx.doi.org/10.1063/1.4870710]

I. INTRODUCTION

Kelvin Probe Force Microscopy (KPFM)[1] imaging is, in its principle, a technique enabling a quantitative determination of the contact potential difference (CPD) between the tip of an atomic force microscope and a sample surface, at the nanoscale. In practice, the *relative* imaging of CPD values is the most common output of KPFM imaging in which a constant CPD level is substracted from the recorded KPFM data. This enables, for example, to compare work functions of different metallic materials on the same sample[2] or to map electrostatic potential drops across electronic devices.[3] While aiming at using KPFM beyond relative imaging purposes, we have shown that the *quantitative* absolute measurement of the CPD between an atomic force microscopy tip and a surface is a tedious work, due to existing instrumental crosstalk effects associated with the use of an ac electrostatic excitation scheme in KPFM, but that such effects may be externally suppressed or compensated.[4]

In this article, we provide a detailed study of the influence of ac cross-talks onto KPFM data. This is of primary importance to determine whether given KPFM measurements are affected or not by such issues. We show in particular that instrumental cross-talks can lead

(i) to artificial CPD shifts with internal parameters of the KPFM set-up, reaching a few Volt range with standard atomic force cantilevers in the 100 kHz frequency range;
(ii) to artificial CPD shifts as a function of the tip-substrate distance, leading to unreliable three-dimensional KPFM mapping, if operated in presence of ac crosstalks;
(iii) and, most important, to an artificial footprint of the sample topography onto KPFM images, even though a constant CPD level is substracted from raw KPFM data.

Experimental results are confronted with a model and simulations. Our work brings a comprehensive view of artefact issues in KPFM imaging, and sheds light on their consequences with respect to quantitative CPD measurements, and to topography footprint issues onto KPFM images. This is of obvious interest for the assessment of the electronic properties of nanomaterials or nanodevices (e.g., nanoscale electronic or photovoltaic devices) in which absolute CPD mapping is required. It is also of strong importance with respect to emerging fields such as KPFM imaging in liquid media or KPFM imaging for biological applications. Cross-talk issues are hence illustrated here on a Tobacco Mosaic Virus (TMV) biological sample.[5–7] Artefact-free KPFM maps are demonstrated and compared with raw instrumental data in presence of ac cross-talks.

II. KPFM MEASUREMENTS IN PRESENCE OF AC CROSS-TALKS

In this section, we describe the principle of KPFM measurements and the expected effect of ac crosstalks onto measured CPD values.[8] We provide results in the case of optical beam atomic force microscopy, and focus on amplitude-modulation KPFM using an ac excitation frequency $\omega/2\pi$ close to the cantilever resonance frequency f_0, assuming an ac + dc electrostatic excitation $V_{dc} + V_{ac}\cos\omega t$ applied to the atomic force microscopy tip. We define, using this convention, the CPD as the dc potential (in Volts) applied to the tip in order to compensate for electrostatic force components

a)Author to whom correspondence should be addressed. Electronic mail: thierry.melin@isen.iemn.univ-lille1.fr

generated by the surface potential V_s (in Volts). V_s can be due, e.g., to a local surface charge (a positive surface charge leads to a positive value of V_s) or to a work-function difference between the tip and surface (a larger sample work-function decreases V_s).[9] The work described hereafter is however not restricted to the usual case of optical beam-deflection amplitude-modulation KPFM, but can be readily extended to frequency-modulation KPFM, to variants of amplitude-modulation KPFM, or to KPFM schemes in which the ac and/or dc excitation are applied to the sample side.

The measurement of the sample surface potential V_s is based: on the detection of the electrostatic force component, $F_\omega(t) = dC/dz\, V_{ac}\,[V_{dc} - V_s] \cos\omega t = F_\omega \cos\omega t$ oscillating at the angular frequency ω in which $C(z)$ is the cantilever tip/substrate capacitance; and on the "nullification" of F_ω as a function of V_{dc} using a feedback-loop, yielding the recorded KPFM signal $V_{dc} = V_s$. In practice, F_ω is measured from the tip oscillation amplitude (amplified output of the photodiode) at the angular frequency ω, of magnitude $A_\omega (> 0)$ and phase φ_ω with respect to the reference ac excitation voltage (see the Fresnel diagram in Fig. 1(a)). The cantilever oscillation vector $(A_\omega; \varphi_\omega)$ is projected on an axis defined by a phase φ (also called "drive phase") with respect to the reference ac excitation. The projected signal $A_\omega \cos(\varphi - \varphi_\omega)$ is used for the KPFM feedback loop since it can be either positive or negative, depending on the sign of $V_{dc} - V_s$, in contrast with A_ω. The feedback loop is built by regulating to zero the projected oscillation amplitude $A_\omega \cos(\varphi - \varphi_\omega)$ as a function of the dc bias component V_{dc}. In this process, in order to minimize the noise level of KPFM measurements, φ can be chosen to match the variations of φ_ω over a $\approx 180°$ range when the excitation angular frequency ω is swept across the cantilever resonance. ω and φ are however only internal parameters of the KPFM measurement, so that the regulated V_{dc} should not depend on the choice of ω and φ, for a correct operation.[4]

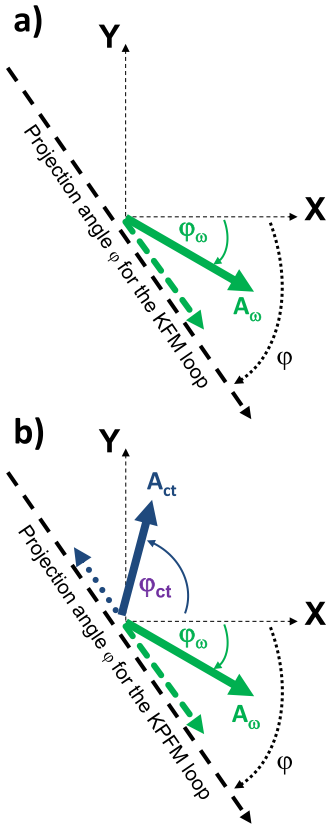

FIG. 1. a) Fresnel diagram showing the cantilever oscillation vector $(A_\omega; \varphi_\omega)$ with respect to the ac electrostatic excitation (X-axis), and its projection (dotted arrow) onto the KFPM feedback loop axis, defined by the angle φ. (b) Fresnel diagram in presence of an ac crosstalk contribution with vector $(A_{ct}; \varphi_{ct})$. Additional crosstalk vectors may be considered in practice (see text).

The effect of an ac-cross-talk in KPFM measurements is shown schematically in Fig. 1(b) by the presence of a spurious oscillation vector $(A_{ct}; \varphi_{ct})$ in the Fresnel diagram $(A_{ct} > 0)$. This cross-talk vector is projected during the KPFM measurement together with the oscillation amplitude $(A_\omega; \varphi_\omega)$, and subsequently affects the measurement of V_{dc}, as visible from Fig. 1(b). This artefact obviously introduces a dependence of the regulated dc potential V_{dc} as a function of the projection angle φ, as well as a dependence with respect to $(A_\omega; \varphi_\omega)$, i.e., the cantilever excitation frequency. In practice, we identified experimentally on our experimental set-ups two sources of ac crosstalks,[4] corresponding on the one hand to a coupling between the ac electrostatic excitation and the photodiode output, hereafter labelled $(A_p; \varphi_p)$; and on the other hand to a coupling between the ac excitation and the piezo actuator ensuring the mechanical excitation of the cantilever during the topography acquisition in tapping mode, labelled $(A_m; \varphi_m)$. The photodiode crosstalk corresponds to a fake cantilever oscillation when read from the photodiode output, while the coupling to the piezo actuator corresponds to a real but spurious mechanical excitation of the cantilever.[4]

The influence of the ac crosstalks on KPFM data can be obtained from the "KPFM equation" corresponding to the nullification of the projection of $(A_\omega; \varphi_\omega)$, $(A_p; \varphi_p)$, and $(A_m; \varphi_m)$ on the axis with angle φ, as illustrated in Fig. 1(b) for a single cross-talk contribution

$$A_\omega \cos(\varphi - \varphi_\omega) + A_p \cos(\varphi - \varphi_p) + A_m \cos(\varphi - \varphi_m) = 0. \tag{1}$$

In this equation, we develop $A_\omega = a_\omega\, dC/dz\, V_{ac}[V_{dc} - V_s]$ (in which a_ω describes the cantilever resonance spectrum) and take $A_p = a_p \cdot V_{ac}$ and $A_m = a_m \cdot V_{ac}$, due to the proportionality of ac cross-talks with V_{ac} (a_m follows here the resonance spectrum of a_ω for $\omega \approx 2\pi f_0$). Developing Eq. (1) leads to the determination of the V_{dc} potential regulated by the KPFM feedback loop

$$V_{dc} = V_s(z) - \underbrace{\frac{a_p}{a_\omega \cdot dC/dz}\left[\frac{\cos(\varphi - \varphi_p)}{\cos(\varphi - \varphi_\omega)}\right]}$$

$$- \underbrace{\frac{a_m}{a_\omega \cdot dC/dz}\left[\frac{\cos(\varphi - \varphi_m)}{\cos(\varphi - \varphi_\omega)}\right]}. \tag{2}$$

This equation shows that the measured KPFM signal consists in the desired surface potential V_s, however with

added artefacts. The two underbraced expressions in Eq. (2) correspond to the two identified ac cross-talks.[4] Equation (2) shows that ac cross-talk artefacts on CPD measurements are z-dependent (via dC/dz at the denominator of ac-cross-talk contributions), and thus interfere with the mapping of V_s as a function of the tip-substrate distance z: This thus prevents, in general, from a reliable 3D KPFM mapping. Equation (2) also points out that even though the ac-crosstalk artefacts are added to V_s, they cannot be simply removed from KPFM maps by a simple surface potential (CPD) offset, unless the tip-substrate capacitance derivative is kept strictly constant during KPFM imaging, which is not the case, in general. In particular, even though V_s may vary as a function of z (e.g., in the case of a surface potential due to a local charge), KPFM images may also exhibit (and be dominated by) an artificial "capacitive footprint" of the sample topography, as due to the variations of dC/dz in Eq. (2) upon sample mapping, and even after substracting a constant CPD offset. This point will be specifically addressed in Sec. V.

In the following, we describe the consequences of ac cross-talks onto KPFM imaging, by confronting the above model to experimental results. The aim is to point out parameters, which affect KPFM measurements, when conducted in presence of ac cross-talks, if a compensation/suppression procedure is not implemented as in Ref. 4. Experiments have been conducted using a Multimode atomic force microscope (Bruker) in ambient air operated with a Nanoscope IIIA/Quadrex electronics or with a Dimension/Nanoscope IV atomic force microscope from the same manufacturer. We scanned either over an Au surface (Secs. III and IV) or over TMV biological samples (Sec. V). Metal-coated cantilever tips have been used in all cases, either with resonance frequency $f_0 \approx 70\,\text{kHz}$ and $k \approx 3\,\text{N/m}$ (EFM PPP, Nanosensors); $f_0 \approx 170\,\text{kHz}$ and $k \approx 5\,\text{N/m}$ (Pt series 14, Mikromasch), and $f_0 \approx 285$–$300\,\text{kHz}$ and $k \approx 40\,\text{N/m}$ (PPP-NCHPt, Nanosensors, or Arrow NCPt, NanoWorld). The amplitude of ac cross-talks has been found to depend on the microscope head (see Sec. III) and to vary linearly with the ac angular frequency ω up to the set-up bandwidths (here, $\approx 400\,\text{kHz}$). KPFM experiments have been performed using a tip-subtrate distance $z \approx 100\,\text{nm}$ (Secs. III and IV) or $z \approx 50\,\text{nm}$ (Sec. V), and an ac excitation amplitude $V_{ac} = 2\,\text{V}$.

III. VARIATION OF CROSS-TALK EFFECTS WITH RESPECT TO KFPM INTERNAL PARAMETERS

We describe in this section the variations of cross-talk effects with respect to KPFM internal parameters (ac excitation frequency ω and KPFM loop projection angle φ). Experimental measurements are confronted with the model of Eq. (2).

A. Increase of cross-talk effects with the ac excitation frequency

The effects of ac cross-talks onto KPFM measurements are first illustrated in Fig. 2, which shows the typical evolution of KPFM signals with respect to the projection angle φ of the KPFM loop. In this figure, we did not systematically show the evolution of KPFM signals with respect to the ac excitation frequency $\omega/2\pi$ in the vicinity of a particular cantilever resonance frequency f_0 (see Ref. 4 or Sec. III C), but rather show KPFM data for a set of three different cantilevers with $f_0 \approx 70\,\text{kHz}$, $f_0 \approx 170\,\text{kHz}$, and $f_0 \approx 300\,\text{kHz}$. The graphs in Fig. 2 illustrate the global increase of ac cross-talk effects with the cantilever oscillation frequency f_0, since ac cross-talks (a_ω) basically linearly increase with the ac excitation frequency. Data also show, on a practical basis, that cross-talk issues easily reach a few Volt scale, and are thus a significant issue for quantitative CPD measurements using standard cantilevers and standard commercial AFMs.

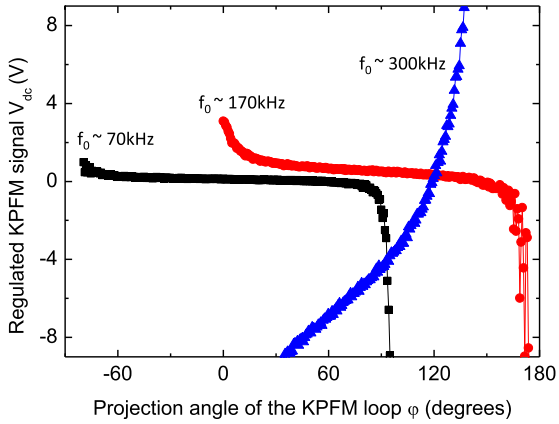

FIG. 2. KPFM measurements on an Au surface plotted as a function of the projection angle φ of the KPFM loop for a set of three cantilevers with increased resonance frequency: $f_0 \approx 70\,\text{kHz}$, $f_0 \approx 170\,\text{kHz}$, and $f_0 \approx 300\,\text{kHz}$.

B. Signatures of ac-cross-talk effects

We describe here the effect of ac cross-talks on the KPFM regulated potential V_{dc} and on the cantilever oscillation signal, as a function of the KPFM projection angle φ and the ac excitation frequency $\omega/2\pi$ or oscillation phase φ_ω. Experimental data have been recorded with a cantilever of resonance frequency $f_0 = 176.8$ kHz excited at $\omega/2\pi = f_0 - 600\,\text{Hz}$ (Fig. 3), or at $\omega/2\pi = f_0 + 400\text{Hz}$ (Fig. 4). Recorded KPFM data consist in the KPFM regulated potential V_{dc}, plotted as a function of the KPFM projection angle φ, and shown in presence of ac cross-talks (black curves in Figs. 3(b) and 3(c) and in Figs. 4(b) and 4(c)), or without ac cross-talks (red curves in Figs. 3(b) and 3(c), and in Figs. 4(b) and 4(c)), as from the procedure of Ref. 4. We also display in Figs. 3 and 4 the residual cantilever oscillation signal A_{err} (output of the photodiode at the angular frequency ω) upon KPFM regulation, which can be viewed as an "error signal" of the KPFM process. This signal is *not*, however, the error signal of the KPFM feedback loop itself, which sets to zero the projection of the cantilever oscillation signal onto the axis with projection angle φ (see Fig. 1), and is assumed here to operate ideally. It rather consists in the amplitude of the cantilever oscillation signal which cannot be set to zero in the projection scheme, i.e., the amplitude of the cantilever oscillation signal orthogonal to the axis with angle φ (see Fig. 1(b)). In absence of ac cross talks, A_{err} is

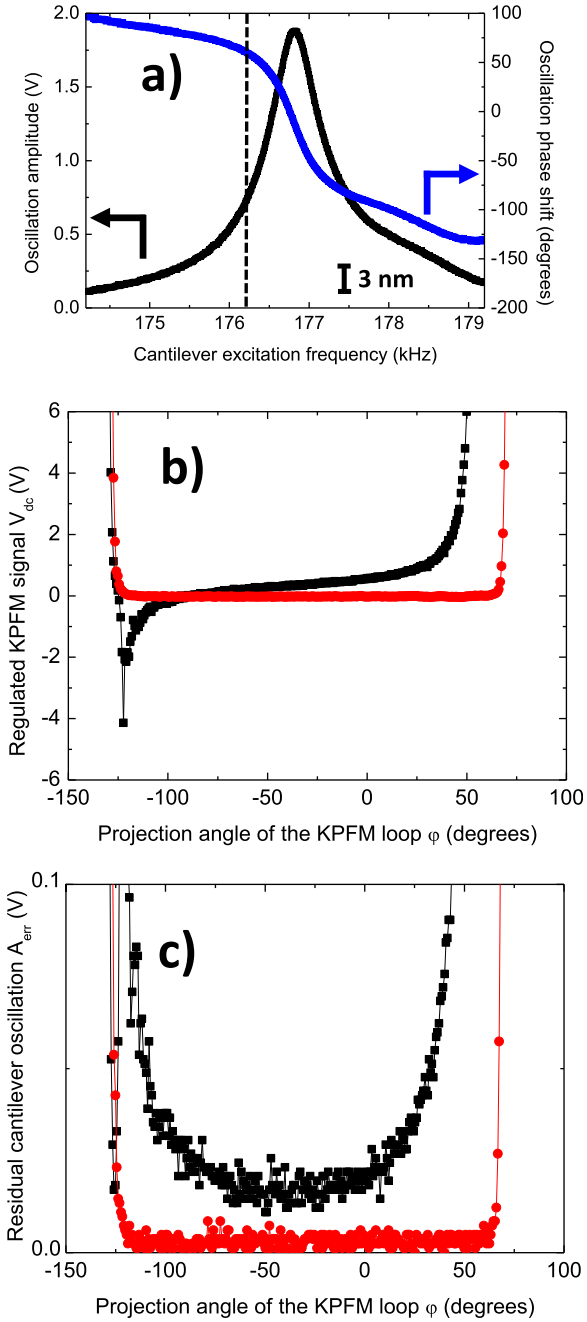

FIG. 3. (a) Cantilever resonance curve (black: amplitude; blue: phase). The cantilever is excited at $\omega/2\pi = 176.2$ kHz (vertical dotted line) in (b) and (c). (b) Regulated KPFM signal V_{dc} plotted as a function of the projection angle φ of the KPFM feedback loop, in presence (black curve) and in absence (red curve) of the instrument ac cross-talks. The feedback loops operates over a $\Delta\varphi \approx 180°$ excursion, and otherwise provides divergent values for V_{dc}. (c) Residual cantilever oscillation signal A_{err}, in presence (black curve) and in absence (red curve) of the instrument ac cross-talks.

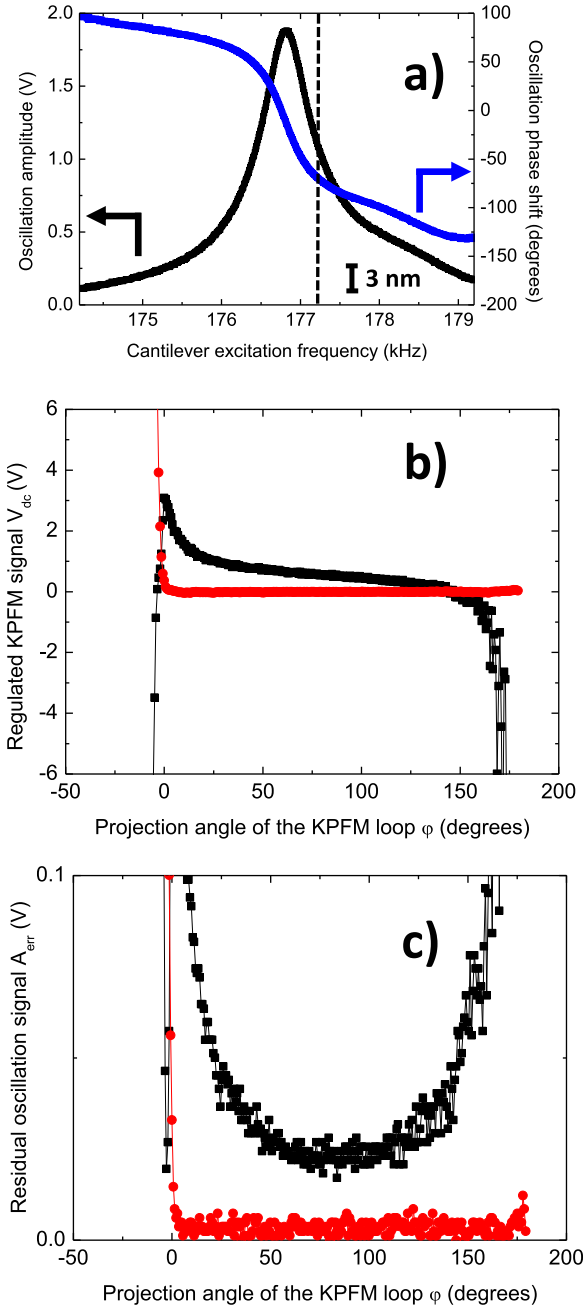

FIG. 4. Same plot as in Figure 3, with the cantilever excited at $\omega/2\pi = 177.2$ kHz in (b) and (c).

by construction equal to zero, irrespective of the value of φ. It is depending on φ otherwise.[10] A_{err} is thus a good indicator of the presence of ac-cross-talks, when plotted as a function of φ. It is therefore also plotted as a function of φ in Figs. 3(c) and 4(c), both in presence of ac cross-talks (black curves), or without ac cross-talks (red curves).

Figs. 3 and 4 show that the regulated KPFM signal V_{dc} exhibits dependences (here at the Volt scale) as a function of φ, and that the residual cantilever oscillation signal A_{err} is non-zero and depends on φ, in presence of ac cross-talks. In these graphs, φ is tuned in a $\Delta\varphi \approx 180°$ range in which the KPFM loop converges (it diverges out of this $\Delta\varphi$ range). It is shown that the suppression/compensation of ac cross-talks[4] provides values of V_{dc}, which are not depending on φ nor on the cantilever ac excitation angular frequency ω (see Figs. 3(b) and 4(b)), and that the residual cantilever oscillation signal A_{err} is also set to zero, irrespective of φ or ω (see Figs. 3(c) and 4(c)). The two features account for a proper operation of the KPFM set-up, and enable a quantitative measurement of the tip-sample CPD, independently of the internal parameters φ or ω.

We finally describe in Fig. 5 the effects of ac cross-talks on the open-loop KPFM amplitude signal, consisting in the cantilever oscillation signal recorded as a function of the dc potential V_{dc}, with the KPFM feedback loop off. In absence of ac cross-talks, this amplitude signal corresponds to A_ω (see Fig. 1(a)) and is thus proportional to $|V_{dc} - V_s|$. It thus exhibits a typical "V-shape," and should be, by construction, zero for $V_{dc} = V_s$. This situation is changed in presence of ac cross-talks since the total cantilever oscillation is the sum of the vectors $(A_\omega; \varphi_\omega)$ and of ac cross-talk contributions noted $(A_{ct}; \varphi_{ct})$ in Fig. 1(b). We plotted in Fig. 5(a) the open-loop KPFM amplitude signal in presence of ac cross-talks, for ac excitations at $\omega/2\pi = f_0 - 600\text{Hz}$ and $\omega/2\pi = f_0 + 400\text{Hz}$, using the same cantilever as in Figs. 3 and 4.[11] The expected "V-shape" as a function of V_{dc} appears rounded, i.e., it exhibits a non-zero minimum value. The extrapolated surface potentials from the plots of Fig. 5(a) also show two distinct values (see vertical dotted lines as guides to the eye). In contrast, the same plots after compensation/suppression of ac cross-talk effects shown in Fig. 5(b) exhibit perfect V-shapes (only the slopes of the cantilever amplitude are different for the two ac excitation frequencies, as due to the change in the cantilever excitation angular frequency ω). In particular, they exhibit a true nullification of the oscillation amplitude as a function of V_{dc}, yielding the same value of the dc potential nullifying the cantilever oscillation signal, unlike in Fig. 5(a). This attests of the proper operation of the KPFM feedback loop.[11]

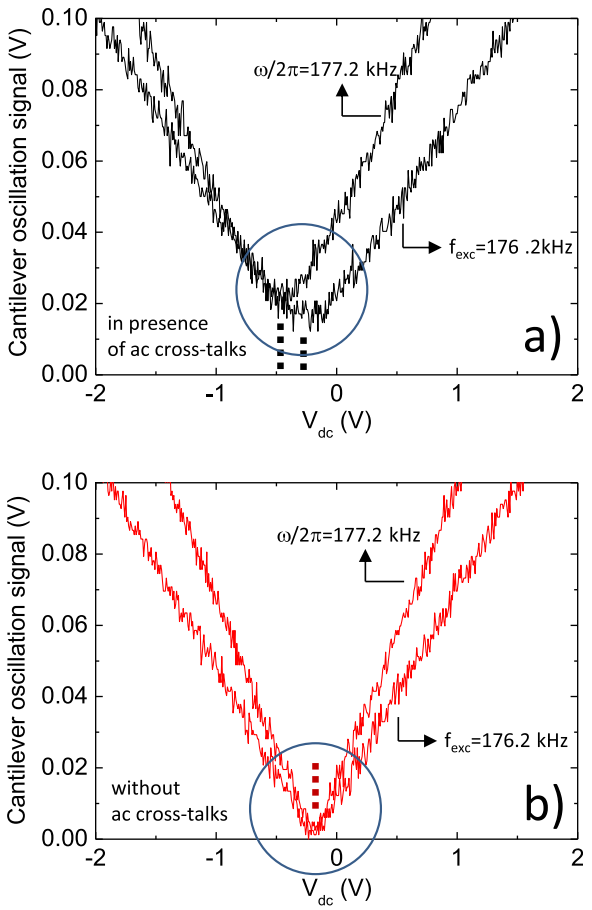

FIG. 5. (a) Cantilever oscillation signal recorded as a function of the dc bias applied to the tip (KPFM feedback loop off), and for the same cantilever as in Figs. 3 and 4, excited either at $\omega/2\pi = 176.2\,\text{kHz}$ and $\omega/2\pi = 177.2\,\text{kHz}$. Both curves correspond to rounded V-shaped curves, due to the presence of instrumental ac cross-talks. The surface potential which would be deduced from these plots is indicated by vertical dotted lines. (b) Same plots, recorded without ac cross-talks. The surface potential is unambiguously defined from the dc potential, which nullifies the cantilever electrostatic oscillation amplitude (see vertical dotted line as a guide to the eye), irrespective of the ac excitation frequency $\omega/2\pi$.

C. Comparison with numerical simulations

We here study the V_{dc} potential regulated by the KPFM loop and the corresponding error amplitude signal A_{err}, in presence of ac cross-talks, and in comparison with the model of Eq. (2). This work is done first in presence of the ac cross-talk to the photodiode solely (first underbraced term in Eq. (2), experimental and simulated data displayed in Fig. 6), and then in presence of both crosstalks (both underbraced terms in Eq. (2), experimental and simulated data displayed in Fig. 7), for sake of comparison.

Experiments have been conducted with a cantilever with $f_0 = 169\,\text{kHz}$. To simulate experimental data from Eq. (2), we characterized the cantilever electrostatic resonance (data not shown), and deduced the value of $a_\omega dC/dz = 0.182\,\text{V}^{-1}$ at f_0, which corresponds to the maximum amplitude of the cantilever electrostatic oscillation (photodiode output, in V) per unit of the ac excitation voltage V_{ac}, and per unit of the dc offset voltage $(V_{dc} - V_s)$. We also determined from the cantilever resonance the experimental value of φ_ω at f_0: $\varphi_\omega = 40°$. The values of $a_\omega dC/dz$ and φ_ω are then described out of the resonance $(\omega/2\pi \neq f_0)$ using an harmonic oscillator model, using the cantilever quality factor $Q = 310$ (as derived from the cantilever electrostatic resonance curve). The cross-talk to the photodiode output has been characterized using an external lock-in by its amplitude and phase $(A_p = a_p \cdot V_{ac}\,;\, \varphi_p)$ with respect to the electrostatic excitation, yielding $a_p = 0.048$ and $\varphi_p = 37°$. We similarly determined the amplitude $A_m = a_m \cdot V_{ac}$ of the mechanical excitation, while its phase φ_m has been adjusted with respect to experimental data in Fig. 7. This gives $a_m = 0.011$ and $\varphi_m = -105°$ at f_0. The behaviour of a_m and φ_m has been described out of resonance using an harmonic model as for a_ω and φ_ω.

The comparison between experimental and simulated KPFM data with the photodiode cross-talk contribution are shown in Fig. 6 in which we plot the KPFM regulated dc bias V_{dc} (Figs. 6(a) and 6(b)) and the residual cantilever oscillation signal A_{err} (Figs. 6(c) and 6(d)) both from experiments and simulations. Each plot in Fig. 6 consists in a set of V_{dc} or A_{err} data as a function of the KPFM feedback loop projection angle φ. The experimental curves (Figs. 6(a) and 6(c)) have been acquired for excitation frequencies between 168 kHz and 170 kHz using steps of 200 Hz. Simulated curves (Figs. 6(b) and 6(d)) also correspond to excitation frequency steps of 200 Hz. Both the set of curves for V_{dc} and A_{err} exhibit similar behaviours between experiments and simulations. In particular, simulations show two distinct nodes marked by vertical arrows in Figs. 6(b) and 6(d) for

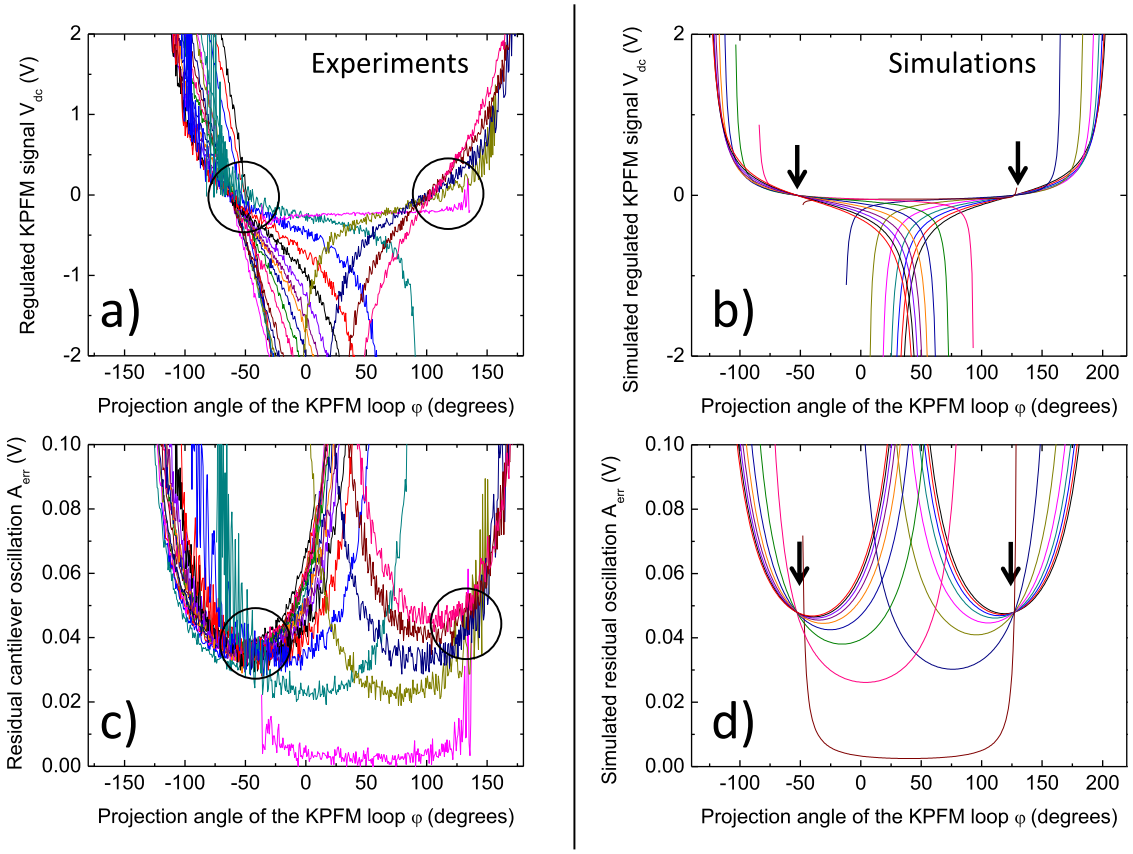

FIG. 6. (a) Experimental values of V_{dc} regulated by the KPFM feedback loop, and plotted as a function of the KPFM feedback loop projection angle φ, for the same type of cantilever as in Figs. 3 and 4. Each curve of the plot corresponds to a different excitation frequency or oscillation phase φ_ω across the cantilever resonance (see text). Experimental data have been acquired in presence of the ac cross-talk to the photodiode, only. (b) Simulated values of the V_{dc} potential regulated by the KPFM feedback loop, using the model of Eq. (2) (see text for the details); (c) Experimental values of the residual cantilever oscillation signal A_{err} during the KPFM feedback loop operation. The curves correspond to the V_{dc} data shown in (a); (d) Simulated values of the residual cantilever oscillation signal A_{err} corresponding to the simulated values of V_{dc} in (b).

which the sets of curves for V_{dc} and A_{err} converge. These nodes correspond to the values of φ falling exactly orthogonal to the ac crosstalk vector $(A_p;\varphi_p)$. This corresponds to $\varphi = \varphi_p \pm 90^\circ$ (nullification of the numerator of the first underbraced term in Eq. (2)), i.e., $\varphi = -53^\circ$ and $\varphi = 127^\circ$. In this configuration, the cross-talk to the photodiode does not interfere with the KPFM feedback loop, so that the KPFM feedback loop output provides $V_{dc} = V_s$, irrespective of the ac excitation frequency. However, the residual on the photodiode A_{err} is not zero although $V_{dc} = V_s$, but equals A_p for each node (here ≈ 0.05 V). Simulation results fall in good agreement with experimental data in which the two nodes can be identified (circles in Figs. 6(a) and 6(c)) with values close to -50° and 130°. Finally, it is seen that a specific value of the excitation frequency leads to A_{err} close to zero irrespective of φ, and corresponds to V_{dc} values almost independent of φ. In this situation, the KPFM feedback loop is insensitive to the internal parameter φ so that V_{dc} seems apparently well-defined. This situation is however peculiar and corresponds to the cantilever oscillation vector parallel to the cross-talk to the photodiode ($\varphi_\omega = \varphi_p$, see the Fresnel diagram in Fig. 1(b)). The value of the regulated dc potential V_{dc} is thus not equal to V_s, but rather to $V_s - a_p/a_\omega dC/dz$, so that the recorded CPD exhibits a fake dependence with respect to the tip-substrate distance z, as will be discussed in the following.

We finally plotted in Fig. 7 the same set of data acquired also in presence of the cross-talk to the mechanical excitation. The set of curves for V_{dc} and A_{err} are now changed. In particular, the two nodes corresponding to $\varphi = \varphi_p \pm 90^\circ$ are washed out to the presence of the second cross-talk contribution. This is due to the fact that the total crosstalk contribution $(A_p;\varphi_p)$ and $(A_m;\varphi_m)$ now explicitly depends on φ since A_m follows the cantilever resonance as a function of ω. As a result, the condition $\varphi = \varphi_p \pm 90^\circ$ cannot be defined irrespective of the excitation frequency ω, which accounts for the disappearance of the nodes at $\varphi = \varphi_p \pm 90^\circ$ in Fig. 7, as compared to Fig. 6. On a general level, the behaviour of V_{dc} and A_{err} is well-reproduced by the simulations in Fig. 7, which fully supports the analysis and model of Eq. (2). Some discrepancies can be observed between the shapes of experimental and simulated curves for V_{dc} and A_{err} in Figs. 6 and 7, but are likely to originate from the non-harmonicity of the actual resonance of the cantilever used in these experiments (see Fig. 3(a) or 4(a)) for sake of illustration). This does not however alter the overall comparison and the validity of the

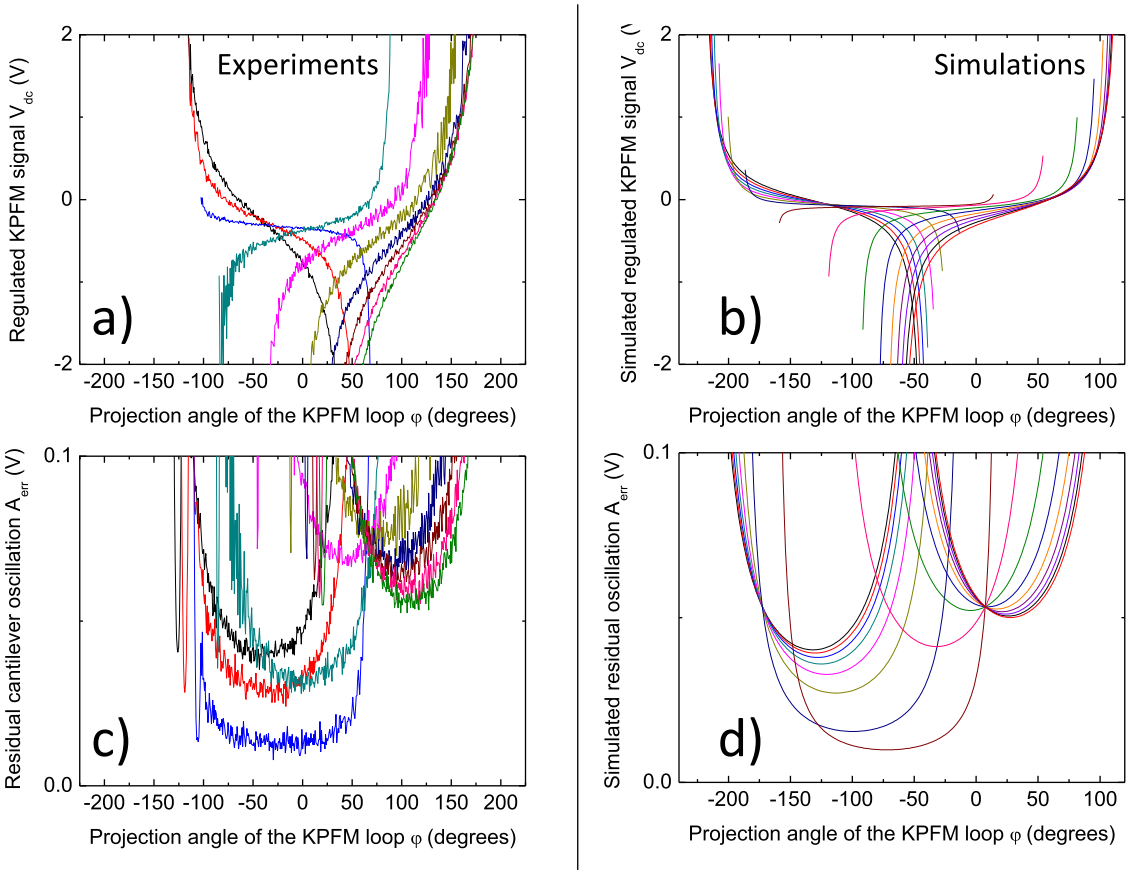

FIG. 7. Same plot as in Fig. 6 but in presence of the photodiode crosstalk and of the cross-talk towards the cantilever mechanical excitation. (a) Experimental values of V_{dc} and (c) simultaneously acquired values of the residual cantilever oscillation signal A_{err} during the KPFM measurement. (b) and (d) Simulations using the model of Eq. (2) (see text).

Eq. (2) to describe ac crosstalk effects onto KPFM measurements.

IV. Z-SPECTROSCOPY OF KPFM SIGNALS IN PRESENCE OF AC CROSS-TALKS

In this section, we illustrate the artefacts introduced by ac cross-talks onto the measurement of the surface potential V_{dc}, as a function of the tip-substrate distance z. This effect hampers the possibility to properly measure a three-dimensional spectroscopy of KPFM signals, even though cross-talk components *do not* depend on z. As can be seen from Eq. (2), this problem is due the normalization of the cross-talk components by the cantilever oscillation amplitude which is proportional to dC/dz. This makes the cross-talk contributions to V_{dc} vary as $(dC/dz)^{-1}$, as seen for each of the underbraced terms in Eq. (2). To illustrate this, we performed KPFM experiments in which we recorded the z-spectroscopy of KPFM signals, and vary artificially the ratio between cross-talk signals towards the photodiode (A_p) and the electrostatic excitation signal (A_ω). This can be done simply, in practice, by moving the laser spot of the atomic force microscopy setup across the cantilever, in order to change the photodiode illumination, and thus to modulate the strength of A_ω versus A_p. To separate the cross-talk effects from the intrinsic evolution with z of the surface potential V_s, we also recorded in Fig. 8(a) the z-spectroscopy of KPFM data recorded by putting the ac + dc bias on the substrate, and in absence of cross-talk contributions. Results are shown in Fig. 8(a) for various laser spot positions across the cantilever. Without noticeable cross-talks (data taken here with the ac + dc bias on the substrate side, triangles in Fig. 8(a)), the z-spectroscopy of KPFM signals does not depend on the laser position along the cantilever. However, in presence of significant cross-talks (data taken with the ac + dc bias on the tip, squares in Fig. 8(a)), the KPFM regulated dc bias V_{dc} exhibits a pronounced dependence on z, which can also be modulated by changing the ratio between A_p and A_ω. This shows that cross-talk effects can play a significant role while probing the z-dependence of KPFM signals.

To demonstrate that the spurious cross-talk contributions induce a well-defined variation of KPFM signals as a function of z, we used the KPFM data from Fig. 8(a) to isolate the cross-talk contributions from the total KFPM signal V_{dc} (underbraced terms in Eq. (2)), and hence to suppress the V_s contribution from the regulated KPFM signal V_{dc}. This is done simply by summing the KPFM data recorded with the ac + dc bias on the tip and with the ac + dc bias on the sample.[12] We then obtain the inverse of the cross-talk contributions to V_{dc} as a function of z, as plotted in Fig. 8(b) in arbitrary units, after normalization for $z = 400\,\text{nm}$. Data show a well-defined decreasing behaviour typical of dC/dz as a function of z, in agreement with Eq. (2). This plot

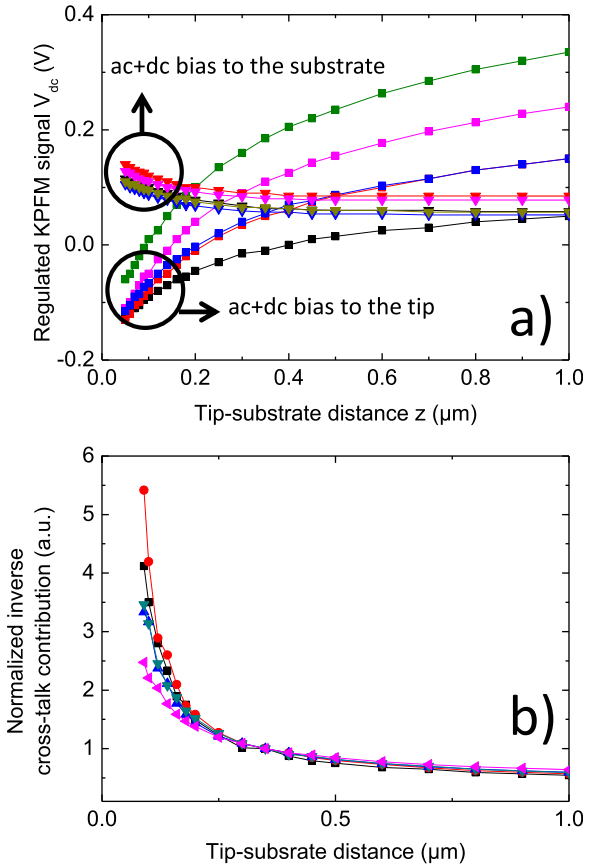

FIG. 8. (a) z-spectroscopy of KPFM data recorded for the ac + dc excitation bias on the tip and for the ac + dc excitation bias on the substrate sides, respectively. The different curves correspond to various positions of the laser spot along the cantilever, resulting in a change of the A_ω ac oscillation signal on the photodiode, while the photodiode ac cross-talk contribution A_p stays constant (see text). (b) Plot of the inverse of the cross-talk contributions to V_{dc} for the four laser spot positions used in (a). The cross-talk contributions are obtained by adding the KPFM signal recorded with the ac + dc bias applied to the cantilever, and the KPFM signal recorded with the ac + dc applied to the sample side. All curves have been normalized for $z = 400$ nm (see text).

demonstrates that the variations of the CPD values as a function of z can be dominated by spurious effects due to ac crosstalks (case of the ac + dc bias on the tip in Fig. 8(a)). The absence of ac cross-talks is therefore a strong requirement with respect to three-dimensional KPFM mapping.

V. KPFM IMAGING ARTEFACTS IN PRESENCE OF AC CROSS-TALKS

We now discuss the effect of dC/dz terms in cross-talk contributions onto KPFM images when acquired with a non-constant capacitance gradient. Artefacts are indeed expected as soon as dC/dz is not constant in a KPFM scan in presence of ac cross-talk, for instance in the usual case of the presence of a nanoscale sample topography. To simplify the discussion, we only refer here to a situation with only a photodiode cross-talk ($A_p \neq 0$ and $A_m = 0$). This situation is obtained using the suppression scheme for A_p as described in Ref. 4. This situation is identical to the case treated in Fig. 6, and discussed in Sec. III C.

To illustrate this point experimentally, and in order to quantify visually the cross-talk effects on KPFM images, we acquired KPFM images on a TMV biological sample. This is to our knowledge the first attempt to record charge distributions along TMVs, beyond early attempts to probe their electric response using piezoresponse force microscopy.[7] TMV is a virus which infects plants (especially tobacco or tomato plants) and is a very stable biological sample, which can be easily deposited on many substrates, and imaged in ambient air by atomic force microscopy.[5] It has also been proposed as a calibration tool in atomic force microscopy since its dimensions are very well defined.[6] Viruses have been deposited on a 300 nm silicon dioxide layer grown on a n-doped silicon substrate, and on a gold-plated silicon substrate, using a protocol described elsewhere.[6] Briefly, a drop of 20 μl of NiCl2 (20 mM) was deposited on the substrates. 2 μl of the TMV sample solution (at 38 nM in 1 mM EDTA) was injected in the drop. After 10 min, the sample was washed with MilliQ water and dried with the help of a vacuum bell and a venturi vacuum pump. KPFM images have been acquired in ambient air conditions. The same scanning parameters were used for all images. The scan size was set to 2×2 μm (256×256 pixels). Images have been acquired at a scan rate of 0.1 Hz, either in constant distance ("lift") mode, or in constant height ("linear") mode, and under Nanoscope 6.14 and Nanoscope 5.1.2 electronics software versions, respectively. Images have been treated with Gwyddion (version 2.34).[13,14]

We first investigate TMVs on silicon dioxide, a situation in which no charge transfer is expected a priori from the substrate to the TMVs. Following the analysis done in Sec. III C and Fig. 6, we conveniently demonstrate the consequence of cross-talks onto KPFM images by comparing the two situations for which: (A) $\varphi_\omega = \varphi_p$ (oscillation vector parallel to the cross-talk vector) or (B) $\varphi = \varphi_p \pm 90^\circ$ (cross-talk vector orthogonal to the projection direction of the KPFM loop). As described in Sec. III C, the situation (A) leads to KPFM images independent of φ but with a maximized (z-dependent) cross-talk contribution; the situation (B) provides images free of cross-talk contributions, the only z-dependence of KPFM signals stemming from the z-dependence of V_s in Eq. (2). Topography and KPFM images of TMVs on silicon dioxide are provided in Fig. 9, with (top) and without (bottom) cross-talk effects, and using in KPFM images either the constant distance ("lift") mode (left set of images) and constant height ("linear") mode (right set of images), with a z tip-offset of 50 nm. In absence of cross-talk effects (bottom images), almost no feature is observable in KPFM images, either acquired in lift or linear mode, which shows that TMVs are not charged nor subjected to a charge transfer from the insulating substrate. The lift-mode KPFM images unambiguously demonstrate that ac cross-talk effects generate a footprint of the sample topography onto KPFM images. This is due to the dC/dz component of the artefact contribution (here, the first underbraced expression in Eq. (2)); and to the fact that in lift-mode, the tip is artificially moved to reproduce the sample topography 50 nm above the surface, therefore inducing artificial local decreases in dC/dz following the sample topography image. This process is illustrated in Fig. 9 in which a

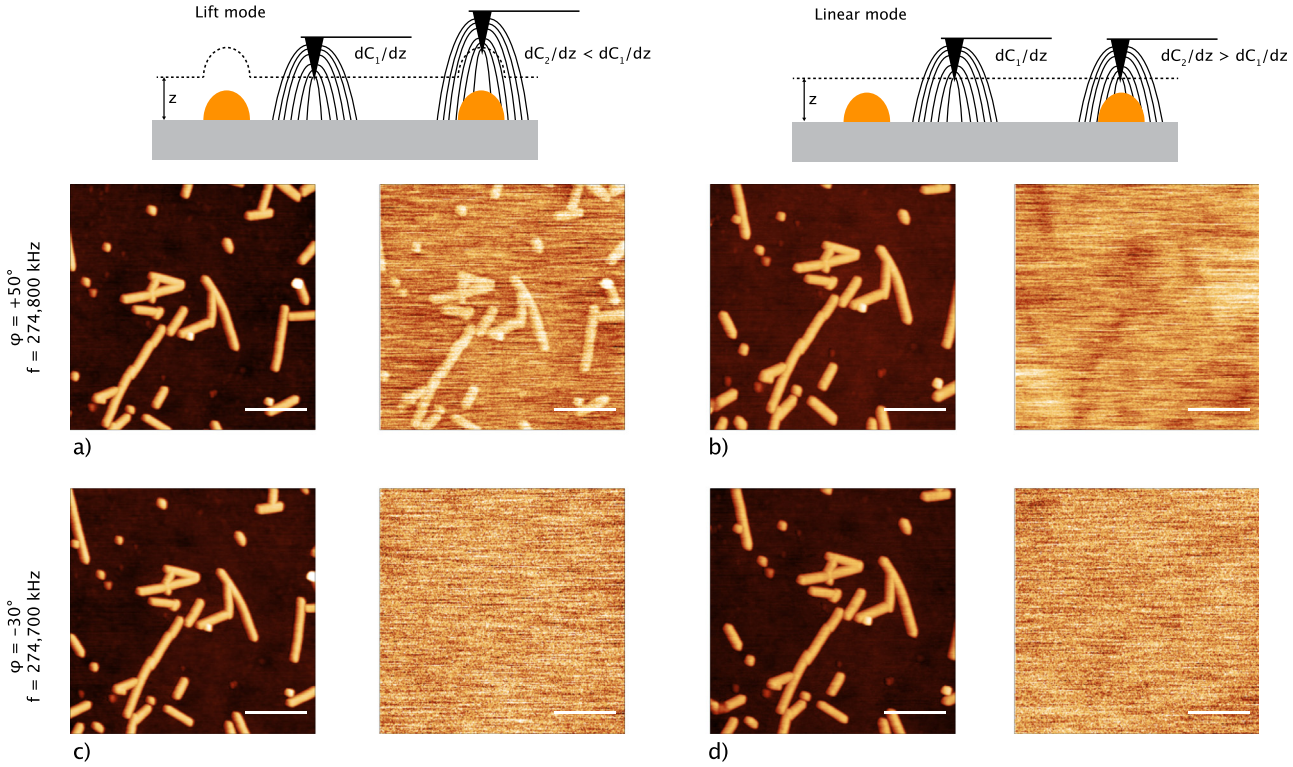

FIG. 9. Topography and KPFM images of tobacco mosaic viruses deposited on silicon dioxide. Scale bars are 500 nm. Colour scales are 25 nm (topography images) and 3 mV (KPFM images). Top: images containing ac cross-talk effects ($\varphi_\omega = \varphi_p$, see text). Bottom: images free of ac cross-talk effects ($\varphi = \varphi_p \pm 90°$, see text). Each couple of images shows the sample topography (left) and the KPFM image (right), acquired with $V_{ac} = 2$ V, and using a z-offset of 50 nm in the lift or linear modes.

topographic feature corresponds to a local increase of the tip-substrate capacitance derivative $|dC_2/dz| < |dC_1/dz|$ in the linear mode, while the artificial replication of the sample topography in the lift mode induces a local decrease of the tip-substrate capacitance derivative ($|dC_2/dz| > |dC_1/dz|$) generated by the imaging mode itself. This obviously replicates the sample topography into the KPFM image in the lift mode. The fake character of the "topographic" KPFM features observed in the lift-mode image in presence of ac cross-talks can also be seen by the fact that the image shows the same lateral resolution as the topography image, although it should contain only long-range Coulomb contributions due to the large z tip-offset. We now examine the corresponding linear mode images (right set of images in Fig. 9). Due to the fact that the tip is here moved parallel to the substrate plane, KPFM images with ac cross-talk effects (Fig. 9(b)) do not show the same direct topography artefact as in the lift mode (Fig. 9(a)). In the linear mode, the change in dC/dz is not dominated by the artificial increase of the tip-substrate distance z (leading to a local decrease in dC/dz) but, rather, to a gradual increase of dC/dz as the tip is moved over a protusion of the sample topography. This leads to the (less-resolved) dark features associated to the TMVs in Fig. 9(b), as compared to the bright features associated with the topography footprint in Fig. 9(a). The linear-mode image of Fig. 9(b) does not display the same spatial resolution as the corresponding topography image, although it is dominated by cross-talk effects induced by the increase of dC/dz when the tip is scanned over the TMVs. This is confirmed by the fact that the linear-mode KPFM image in absence of cross-talk contributions (Fig. 9(d)) is identical to the lift-mode image (Fig. 9(c)), showing here no charging of the TMVs on silicon dioxide.

We finally examined the case of TMVs deposited on a gold-plated n-doped silicon substrate. Topography and KPFM images are shown in Fig. 10 in which we directly used scanning conditions for which $\varphi = \varphi_p \pm 90°$ (cross-talk vector orthogonal to the projection direction of the KPFM loop, no topography artefacts due to ac cross-talks). Images are shown both for $\varphi = \varphi_p + 90°$ (top) and $\varphi = \varphi_p - 90°$ (bottom), and both in lift and linear modes (left and right sets of images, respectively). Both sets of images for $\varphi = \varphi_p \pm 90°$ are almost identical, except for the signal to noise ratios, which are different due to the use of different excitation frequencies. Although cross-talk effects have been suppressed, both lift-mode images (Figs. 10(a) and 10(c)) display a topography footprint effect, as due to an explicit z-dependence of the surface potential V_s. As a result, the use of the lift-mode for KPFM imaging—which artificially reproduces the sample topography above the surface—also induces an artificial variation of the recorded V_s following the sample topography, leading to the observed topography footprint. This footprint is avoided while imaging in the linear mode image shown in Figs. 10(b) and 10(d) in which the TMVs are imaged as dark features, which evidences a negative charge transfer from the Au substrate towards the TMVs. It is also seen that the amplitudes of KPFM signals in the image in Figs. 10(b) and 10(d) do not strictly correlate with the TMV topography, i.e., the TMV charging is not homogeneous along the TMV particles. This point is a clear

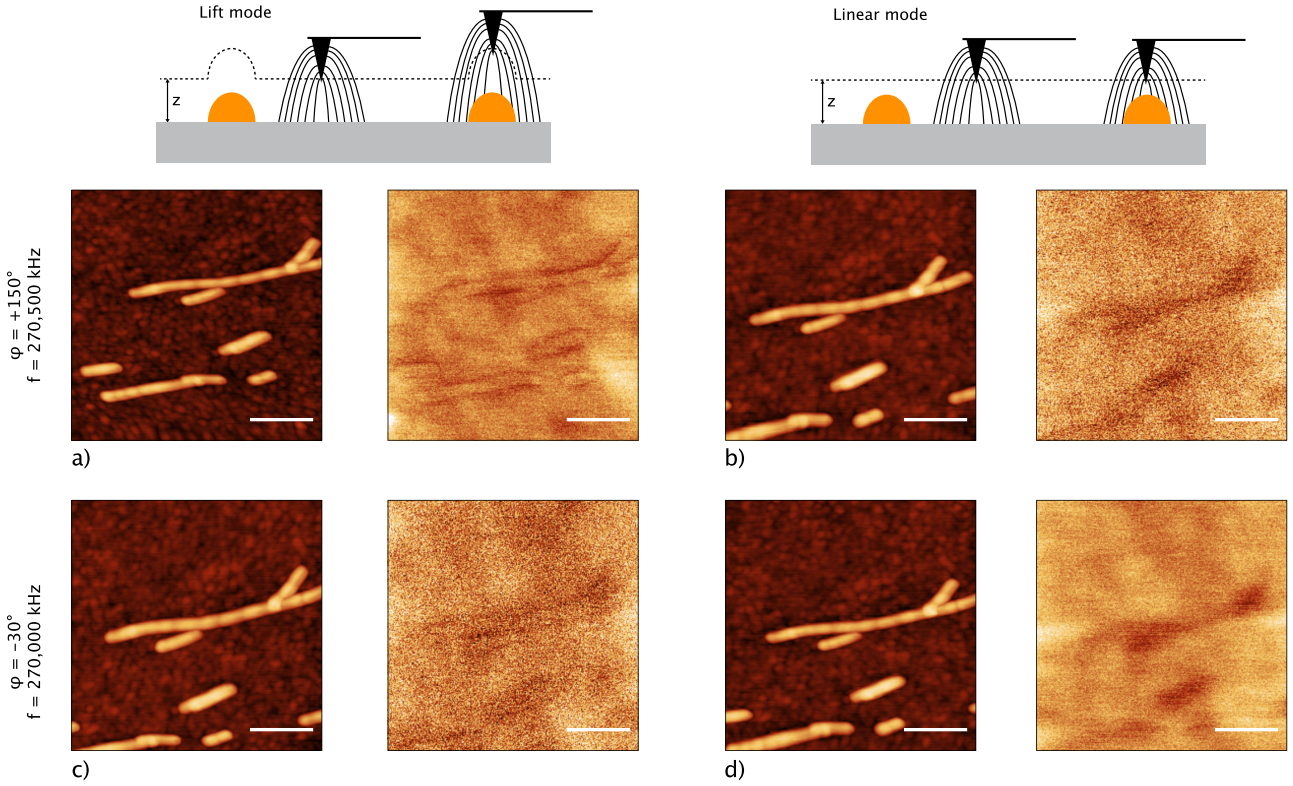

FIG. 10. Topography and KPFM images of tobacco mosaic viruses deposited on Au-plated silicon. Scale bars are 500 nm. Colour scales are 25 nm (topography images) and 30 mV (KPFM images). Images in this figure have been taken without ac cross-talk effects (cross-talk vector orthogonal to the KPFM projection angle), and for $\varphi = \varphi_p + 90^\circ$ (top) and for $\varphi = \varphi_p - 90^\circ$ (bottom). Each couple of images shows the sample topography (left) and the KPFM image (right), acquired with $V_{ac} = 2$ V, and using a z-offset of 50 nm in the lift or linear modes. Linear mode images ((b) and (d)) show the charge transfers between the Au substrate and the TMVs.

indication that the linear mode KPFM imaging of the TMVs has been properly achieved and is not subjected to any artefact.

VI. CONCLUSION

In conclusion, we have provided in this paper a comprehensive study of ac cross-talk effects onto KPFM imaging. Such effects manifest first by a dependence of regulated KPFM signals as a function of the KPFM set-up internal parameters, such as the cantilever excitation frequency $\omega/2\pi$ and the projection angle φ of the KPFM feedback loop. They also induce a fake dependence of the measured KPFM signals as a function of the tip-substrate distance z, thus preventing, if present in experiments, from a reliable spectroscopy of KPFM signals as a function of z, and hence, from the possibility to perform a three-dimensional KPFM imaging. It was also shown that ac cross-talks additionally generate imaging artefacts in the form of topography footprints onto KPFM images, especially in constant distance (lift) modes of imaging. This point was unambiguously demonstrated, taking as an example the case of KPFM imaging of tobacco mosaic virus samples on insulators and metal substrates. Instrumental ac cross-talks should therefore be carefully considered in KPFM techniques requiring large ac frequencies, such as amplitude-modulation KPFM, or, e.g., frequency-modulation KPFM in liquid environments.

ACKNOWLEDGMENTS

This work has been achieved using the facilities of the EXCELSIOR Nanoscience Characterization Center and of the RENATECH program and was, in part, supported by the French National Research Agency under Contract No. ANR-11-BS10-0004. We thank Dr. Jean-Luc Pellequer (CEA Marcoule, DSV/iBEB/SBTN, F-30207 Bagnols-sur-Cèze, France) for providing us with the TMV sample. M.P. would like to acknowledge Michael Odorico and Professor Pierre Parot and the training school provided by the COST Action TD1002 AFM4NanoMed & Bio.

[1]Y. Martin, D. W. Abraham, and H. K. Wickramasinghe, Appl. Phys. Lett. **52**, 1103 (1988); M. Nonnenmacher, M. P. O'Boyle, and H. K. Wickramasinghe, *ibid.* **58**, 2921 (1991).
[2]X. Cui, M. Freitag, R. Martel, L. Brus, and P. Avouris, Nano Lett. **3**, 783–787 (2003); N. Gaillard, M. Gros-Jean, D. Mariolle, F. Bertin, and A. Bsiesy, Appl. Phys. Lett. **89**, 154101 (2006); S. Barbet, R. Aubry, M.-A. di Forte-Poisson, J.-C. Jacquet, D. Deresmes, T. Mélin, and D. Théron, *ibid.* **93**, 212107 (2008).
[3]S. H. Charrier, M. Kemerink, B. E. Smalbrugge, T. de Vries, and R. A. J. Janssen, ACS Nano **2**, 622 (2008); D. Brunel, D. Deresmes, and T. Mélin, Appl. Phys. Lett. **94**, 223508 (2009).
[4]T. Mélin, S. Barbet, H. Diesinger, D. Théron, and D. Deresmes, Rev. Sci. Instrum. **82**, 036101 (2011); H. Diesinger, D. Deresmes, J.-P. Nys, and T. Mélin, Ultramicroscopy **108**(8), 773–781 (2008).
[5]Y. G. Kuznetsov and A. McPherson, Microbiol. Mol. Biol. Rev. **75**, 268 (2011).

[6]M.-H. Trinh, M. Odorico, L. Bellanger, M. Jacquemond, P. Parot, and J.-L. Pellequer, J. Mol. Recogn. **24**, 503 (2011).
[7]S. V. Kalinin, S. Jesse, W. Liu, and A. A. Balandin, Appl. Phys. Lett. **88**, 153902 (2006).
[8]Previous studies have discussed the effect of a KPFM regulation on a non-zero amplitude (not relevant here): see Y. Wu and M. A. Shannon, Rev. Sci. Instrum. **77**, 043711 (2006).
[9]The CPD may be alternatively defined as the opposite of V_s. In that case, a larger sample work function will lead to a larger measured CPD value, while a positive charge distribution at the sample will decrease the CPD.
[10]The error signal A_{err} can be calculated as $A_{err} = |A_p \sin(\varphi - \varphi_p) + A_m \sin(\varphi - \varphi_m) + A_\omega \sin(\varphi - \varphi_\omega)|$ and using the condition provided by the KPFM regulation loop in Eq. (1), and leading analytically to: $A_{err} = |A_p \sin(\varphi_p - \varphi_w)/\cos(\varphi - \varphi_w) + A_m \sin(\varphi_m - \varphi_w)/\cos(\varphi - \varphi_w)|$. This analytical approach may be used in practice for a photodiode cross-talk solely ($A_m = 0$), since A_m and φ_m are varying with the excitation frequency ω (i.e., with φ_ω) across the cantilever resonance.
[11]The CPD values nullifying the cantilever oscillation signal in Fig. 5(b) are seen to differ from the KPFM regulated dc values in Figs. 3(b) and 4(b). The two experiments have been carried out separately. The difference in CPD corresponds here likely to a tip or surface change between the two set of experiments and is not related to the instrumentation.
[12]This approach is valid if the analog to digital cards through which KPFM data are recorded do not exhibit significant offsets. Such offsets have been measured in the few tens of mV range on our setups.
[13]For the height images, the following filters were used: plane level, median line correction, minimal value was set to 0, and the scale bars were all set between 0 and 25 nm. For the potential images, the following filters were used: plane level; median line correction. The scales were adapted to the values of the measured potentials. The scale bars were added with matplotlib (version 1.3.1); J. D. Hunter, Comput. Sci. Eng. **9**, 90 (2007).
[14]D. Nečas and P. Klapetek, Central Eur. J. Phys. **10**, 182–188 (2012).